JACS
JOURNAL OF THE AMERICAN CHEMICAL SOCIETY
pubs.acs.org/JACS
Article

An Unconventional Dark Radical Chemistry in Dense Molecular Clouds: Directed Gas-Phase Formation of Naphthyl Radicals

Zhenghai Yang, Galiya R. Galimova, Chao He, Shane J. Goettl, Xiaohu Li,* Alexander M. Mebel,* and Ralf I. Kaiser*

Cite This: J. Am. Chem. Soc. 2025, 147, 47359−47369
Read Online
ACCESS | Metrics & More | Article Recommendations | Supporting Information

ABSTRACT: The synthetic pathways to aromatic molecules inside photon-shielded dense molecular clouds remain a fundamental, unsolved enigma in astrochemistry and astrophysics, with low-temperature molecular growth routes involving aromatic radicals, such as prototype bicyclic naphthyl ($C_{10}H_7^{\bullet}$), implicated as key sources. Here, exploiting crossed molecular beam experiments augmented by electronic structure calculations, unexpected pathways are exposed leading to the gas-phase formation of 1- and 2-naphthyl via barrierless bimolecular reactions of atomic carbon (C) with indene (C_9H_8) and of dicarbon (C_2) with styrene (C_8H_8) accompanied by ring expansion and cyclization together with aromatization. These facile routes challenge conventional wisdom that aromatic radicals are formed in deep space solely via "bright" gas-phase photochemistry of their closed-shell polycyclic aromatic hydrocarbon (PAH) precursors. A hitherto disregarded "dark" aromatic radical chemistry with aromatic radicals synthesized via gas-phase reactions offers new concepts on the chemical evolution of the chemistry of dark molecular clouds eventually culminating in the rapid formation of aromatics, fullerenes, and carbonaceous nanostructures.

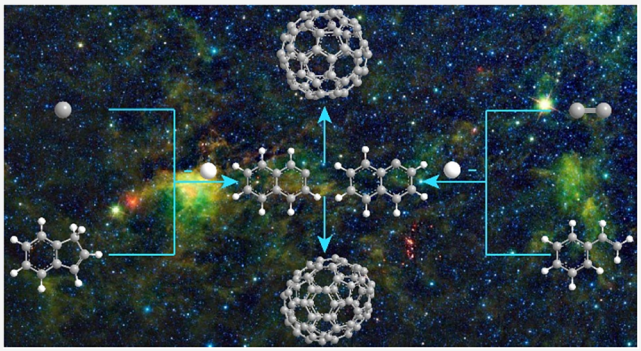

1. INTRODUCTION

The ubiquitous presence of polycyclic aromatic hydrocarbons (PAHs)—organic molecules composed of fused benzene rings—along with their derivatives such as hydrogenated, ionized, and substituted counterparts in the interstellar medium and in carbonaceous chondrites like Orgueil, Allende, and Murchison has remained a key paradox in our Universe considering that interstellar PAHs are faster destroyed than synthesized.[1−6] Accounting for up to 20% of the galactic carbon budget, rapid and barrierless bimolecular reactions commencing with prototype mono- (phenyl, $C_6H_5^{\bullet}$)[7] and bicyclic (1-/2-naphthyl, $C_{10}H_7^{\bullet}$) aromatic radicals[8] signify critical molecular mass growth processes to aromatic molecules in cold molecular clouds at temperatures as low as 10 K, thus affording a sustainable solution to this puzzle. In particular, naphthalene ($C_{10}H_8$) and anthracene/phenanthrene ($C_{14}H_{10}$) can be prepared in the gas phase through the reactions of phenyl and 1-/2-naphthyl radicals, respectively, with vinylacetylene (C_4H_4) via the hydrogen abstraction−vinylacetylene addition (HAVA) mechanism.[7−9] Except for the key role in forming acenes, helicenes, and phenacenes with fused benzene rings,[8,10] naphthyl radicals ($C_{10}H_7^{\bullet}$) have also emerged as fundamental precursors to acenaphthylene ($C_{12}H_8$),[11] fluorene ($C_{13}H_{10}$),[12] and fluoranthene ($C_{16}H_{10}$)[13] carrying five-membered rings, which represent critical molecular building blocks to nonplanar PAHs like corannulene and even fullerenes (Figure S1).[12,13] This classifies naphthyl radicals as central reaction intermediates in molecular mass growth processes to two- (2D) and three-dimensional (3D) carbonaceous nanostructures in deep space. Recently, mechanisms on distinct carbonaceous particle formation stages, especially the soot inception stage, were also explored.[14−17]

The recent detection of PAHs carrying up to four six-membered rings in the returned samples from the carbonaceous asteroids Ryugu[18,19] and Bennu[20,21] within the framework of the OSIRIS-REx mission suggest a hitherto unidentified low-temperature reservoir of aromatic molecules, which cannot be supported by the previously contemplated classical photolysis driven formation of reactive aromatic radicals like phenyl ($C_6H_5^{\bullet}$) and naphthyl ($C_{10}H_7^{\bullet}$) within cold molecular clouds. However, which mechanisms can be proposed to account for the formation of interstellar naphthyl radicals? While ultraviolet (UV) photolysis of naphthalene

Received: September 4, 2025
Revised: November 11, 2025
Accepted: December 4, 2025
Published: December 13, 2025

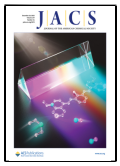

https://doi.org/10.1021/jacs.5c15459
J. Am. Chem. Soc. 2025, 147, 47359−47369

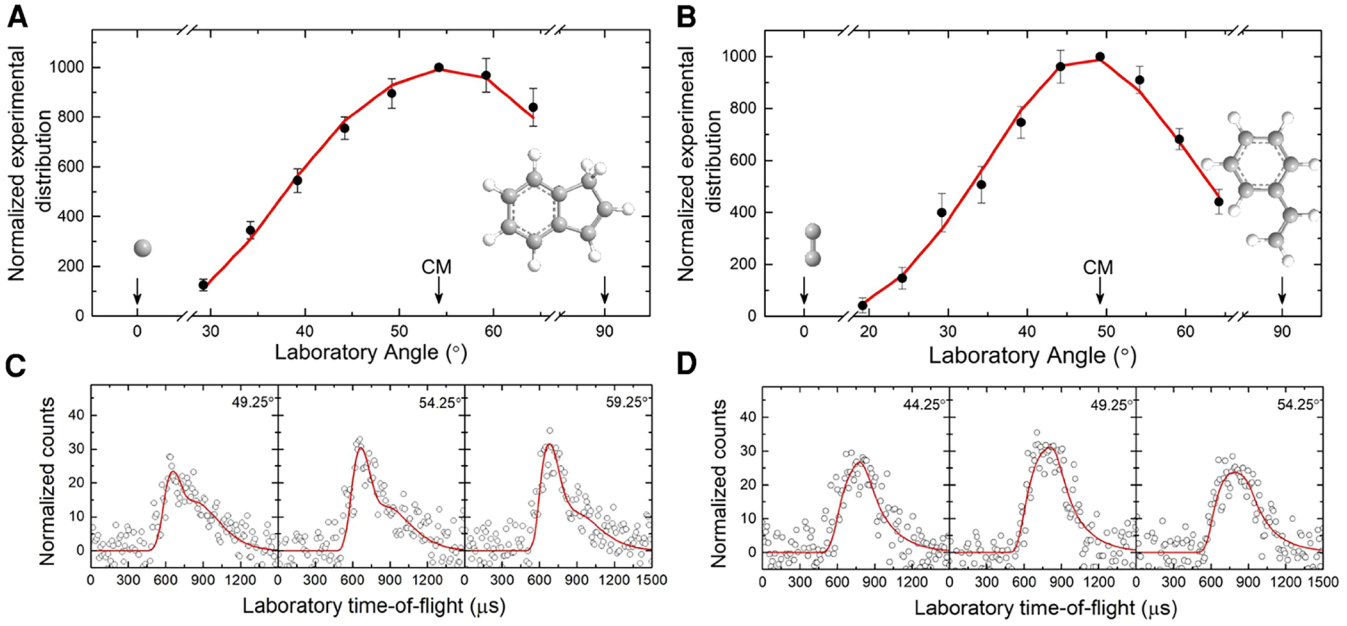

Figure 1. LAD (A, B) and TOFs (C, D) for the reactions of atomic carbon with indene (A, C) and dicarbon molecule with styrene (B, D). The solid circles with their error bars represent the normalized experimental distribution; the open circles indicate the experimental data. The red lines represent the best fits obtained. Atoms are color-coded in gray (carbon) and white (hydrogen).

($C_{10}H_8$) preferentially leads to atomic hydrogen loss forming naphthyl radicals ($C_{10}H_7^{\bullet}$),[2] UV photons from the ambient interstellar radiation cannot reach the dense, inner regions of cold molecular clouds with the strength of photon field reduced at least by a factor of 10^3.[22−24] A cosmic ray induced internal UV field present even deep inside cold molecular clouds could be too weak to drive an efficient photodissociation network and sufficient fractional abundances of polycyclic aromatic radicals such as naphthyl radicals ($C_{10}H_7^{\bullet}$) as the prototype representative.[25,26] Therefore, "bright" mechanisms leading to PAH radicals via photolysis of closed-shell PAHs have not been able to fully account for a plethora of aromatics detected on Ryugu[18,19] and Bennu.[20,21] Low-temperature bimolecular gas-phase routes to naphthyl radicals ($C_{10}H_7^{\bullet}$) and to other PAH radicals from astrochemically relevant reactants in general may afford an elegant and versatile "dark" reservoir of PAH radicals such as naphthyl ($C_{10}H_7^{\bullet}$) *without* the need of photon-initiated molecular mass growth processes even in the darkest and coldest molecular clouds.[27]

The molecular beam technique represents a unique tool in understanding chemical reactions and the underlying mechanisms on the molecular level. In particular, the crossed molecular beam (CMB) method coupled with universal mass spectrometric detection of the products allows us to unravel the formation routes to complex molecules, including transient species in combustion flames and low-temperature environments of cold molecular clouds. Here, utilizing a universal CMB machine, we report the very first directed gas-phase synthesis of 1- and 2-naphthyl radicals ($C_{10}H_7^{\bullet}$, X^2A') via the bimolecular reactions of ground-state atomic carbon (C, ^3P) with indene (C_9H_8, X^1A') (reaction 1) and of dicarbon molecule (C_2, $X^1\Sigma_g^+/a^3\Pi_u$) with styrene ($C_6H_5C_2H_3$, X^1A') (reaction 2) under single-collision conditions. Carbon and dicarbon beams are produced via laser ablation of a rotating graphite rod and seeding the ablated species in noble gases, whereas Krypton-seeded styrene and indene molecular beams are generated in the secondary source (Figures S2 and S3, Supporting Information). As demonstrated by the electronic structure calculations, both reactions appeared to be barrierless and exoergic thus providing facile routes to interstellar naphthyl radicals via two distinct pathways involving ring expansion (reaction 1) and cyclization along with aromatization (reaction (2)) even in the darkest regions of molecular clouds from readily available organic reactants in these C1+C9 (carbon−indene) and C2+C8 (dicarbon−styrene) systems at 10 K. These findings challenge conventional wisdom that molecular mass growth processes in molecular clouds must be initiated via photolysis of closed-shell gas-phase PAHs through a "bright" chemistry, thus affording a viable alternative of a "dark" chemistry initiated through bimolecular reactions leading to aryl radicals, fundamentally enhancing our understanding of the chemical evolution of the aromatic Universe we live in.

$$C(12\ \text{amu}) + C_9H_8(116\ \text{amu}) \rightarrow C_{10}H_7^{\bullet}\ (127\ \text{amu}) + H(1\ \text{amu}) \quad (1)$$

$$C_2(24\ \text{amu}) + C_8H_8(104\ \text{amu}) \rightarrow C_{10}H_7^{\bullet}(127\ \text{amu}) + H(1\ \text{amu}) \quad (2)$$

2. RESULTS

2.1. Carbon−Indene and Dicarbon−Styrene Systems—Laboratory Frame. The reactive scattering experiments (1) and (2) were carried out in the gas phase under single-collision conditions (Methods) (Figure 1). In the atomic carbon (C, ^3P)−indene (C_9H_8, X^1A') system, a reactive scattering signal was observed at mass-to-charge (m/z) ratios of 127 ($C_{10}H_7^+/^{13}CC_9H_6^+$) and 126 ($C_{10}H_6^+/^{13}CC_9H_5^+$). Compared to m/z = 127, the relative intensity of the TOF spectra recorded at m/z = 126 was only 0.38 ± 0.03, with TOF spectra at both m/z values indistinguishable after scaling. These findings hint that the signal at m/z = 127 originated

https://doi.org/10.1021/jacs.5c15459
J. Am. Chem. Soc. 2025, 147, 47359−47369

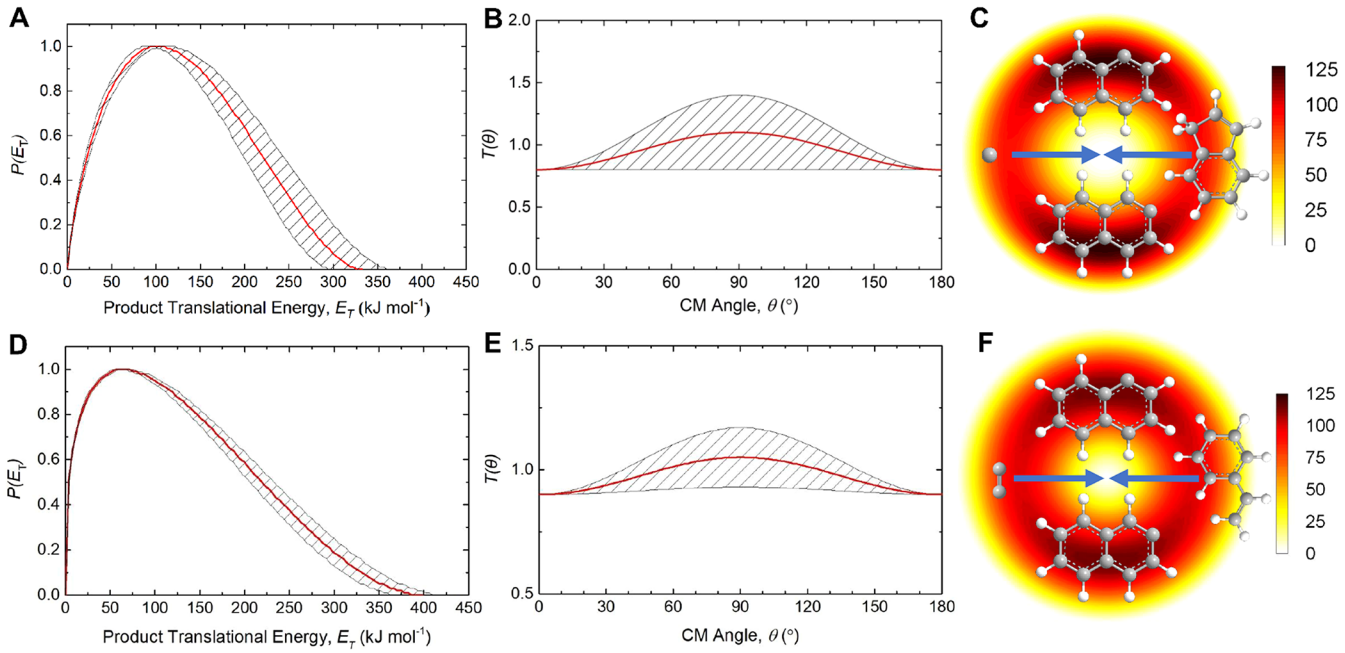

Figure 2. CM translational energy (A, D), angular flux distributions (B, E), and the flux contour map (C, F) for the reaction of atomic carbon with indene (A–C) and dicarbon molecule with styrene (D–F). The solid red lines and shaded areas define the best fit and the error limits, respectively.

from the formation of $C_{10}H_7^{\bullet}$ radicals (127 amu) along with atomic hydrogen (1 amu), with ion counts at m/z = 126 associated with dissociative ionization of the parent species at m/z = 127. Considering the enhanced signal-to-noise (S/N) ratio at m/z = 127 compared to m/z = 126, TOF spectra were recorded at m/z = 127 from 30° to 65° in 5° intervals. These TOF spectra were then integrated to obtain the laboratory angular distribution (LAD) (Figure 1A,B). The LAD is essentially forward–backward symmetric and displays a maximum around the CM angle; this finding implies indirect scattering dynamics[28] and the formation of long-lived $C_{10}H_8$ complex(es)[29] ultimately decomposing via hydrogen elimination to $C_{10}H_7^{\bullet}$ product(s). Therefore, our experimental data alone reveal the atomic carbon versus atomic hydrogen exchange pathway, resulting in the gas-phase preparation of $C_{10}H_7^{\bullet}$ isomer(s) in the carbon–indene system.

In the case of the dicarbon (C_2, $X^1\Sigma_g^+/a^3\Pi_u$)–styrene (C_8H_8, X^1A') system (reaction 2), reactive scattering signal was also detected at m/z = 127 and 126. In analogy to reaction 1, TOF data at m/z = 127 and 126 overlapped after scaling. Considering the better signal-to-noise (S/N) ratio at m/z = 127 as compared to m/z = 126, with relative intensities of 1.00:0.62 ± 0.03, TOF data were collected at m/z = 127 over a range of 50° in 5° intervals. Once again, the forward–backward symmetric LAD along with the detected mass-to-charge ratios alone provide evidence on the gas phase formation of $C_{10}H_7^{\bullet}$ (127 amu) isomer(s) along with atomic hydrogen (1 amu) via reaction 2 involving long-lived $C_{10}H_8$ intermediates (indirect scattering dynamics) (Figure 1). Additional information on the position where the hydrogen loss originates from, i.e., the aromatic ring and/or the vinyl moiety, can be obtained by conducting experiments of dicarbon with D3-($C_6H_5C_2D_3$) and D5-styrene ($C_6D_5C_2H_3$). For the C_2-$C_6H_5C_2D_3$ system, signal was probed at m/z = 130 ($C_{10}H_4D_3^+$) and 129 ($C_{10}H_3D_3^+/C_{10}H_5D_2^+$) with the determined ratio of 1:1.22 ± 0.03, taking into account the contribution of natural ^{13}C isotopes and differences of the spread recoil circles of the atomic hydrogen versus deuterium loss. For the C_2-$C_6D_5C_2H_3$ system, a ratio of 1 (m/z = 132): 0.78 ± 0.02 (m/z = 131) is obtained. These results expose that the atomic hydrogen loss can originate from both the vinyl moiety *and* the phenyl group (Supporting Information).

2.2. Carbon–Indene and Dicarbon–Styrene Systems—Center-of-Mass Frame. The compelling identification of $C_{10}H_7^{\bullet}$ isomer(s) in both the carbon–indene and dicarbon–styrene systems affords an elucidation of the nature of the isomer(s) along with the underlying mechanisms. This is achieved by converting the laboratory data (TOFs, LAD) into the center-of-mass reference frame yielding the translational energy ($P(E_T)$) and angular flux ($T(\theta)$) distributions (Figure 2).[30] *First*, for both systems, best fits of the laboratory data are derived via a single atomic hydrogen loss channel involving reactions 1 and2. For the carbon–indene system (Figure 2A,B), the $P(E_T)$ function is characterized by a distribution maximum of 101 ± 9 kJ mol^{-1}, suggesting a tight exit transition state upon the unimolecular decomposition of the $C_{10}H_8$ complex(es). Further, a high-energy cutoff of E_{max} = 328 ± 33 kJ mol^{-1}, which represents the sum of the reaction exoergicity plus the collision energy (35.8 ± 1.2 kJ mol^{-1}), is extracted for those products formed without internal excitation. This results in an exoergic reaction of 293 ± 34 kJ mol^{-1}. For the dicarbon–styrene reaction (Figure 2D,E), a distribution maximum of the $P(E_T)$ was also observed here at 66 ± 4 kJ mol^{-1}, which also indicates a tight exit transition state involving significant reorganization of the electron density upon decomposition of the $C_{10}H_8$ intermediates to the separated products. A E_{max} of 384 ± 23 kJ mol^{-1} is revealed; considering the collision energy of 20.6 ± 0.5 kJ mol^{-1}, reaction energies of −363 ± 23 kJ mol^{-1} and −371 ± 23 kJ mol^{-1} for dicarbon reactants in their $X^1\Sigma_g^+$ ground state and $a^3\Pi_u$ excited state, respectively, are extracted. Fractions of 39 ± 7% and of 34 ± 4% of the available energy channeling into the translation degrees of freedom of the products are observed for reactions (1) and (2), respectively,

https://doi.org/10.1021/jacs.5c15459
J. Am. Chem. Soc. 2025, 147, 47359–47369

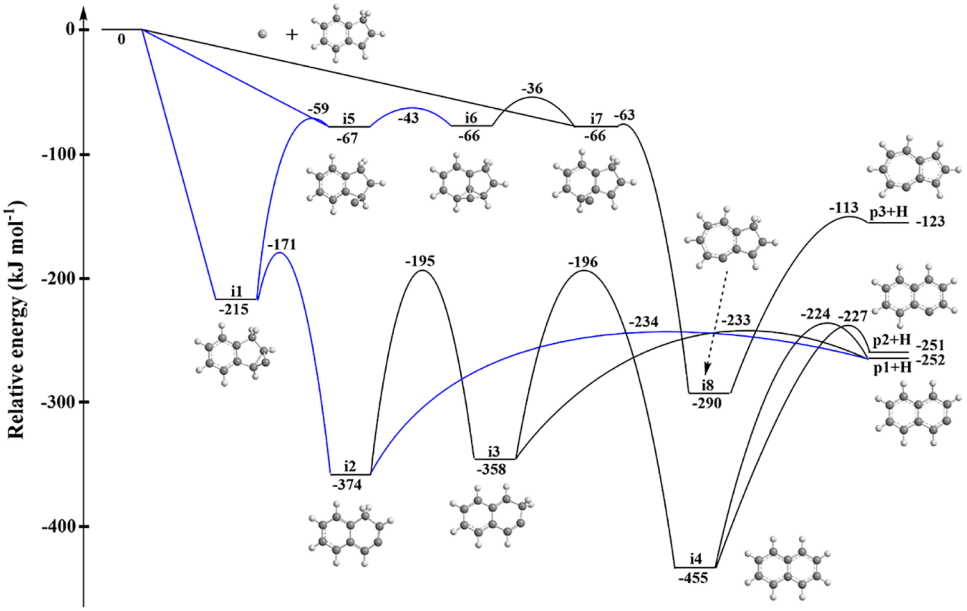

Figure 3. Triplet potential energy surface (PES) for the reaction of atomic carbon (C, ^{3}P) with indene (C_9H_8). The pathway highlighted in blue represents the dominant routes to naphthyl radicals.

also supporting indirect scattering dynamics.[29] *Second*, the $T(\theta)$ functions exhibit a forward−backward symmetric pattern and peak intensities at 90° (sideway scattering). These findings reveal indirect dynamics involving the formation of the $C_{10}H_8$ intermediates holding a lifetime that is comparable to or exceeding their rotational period.[31] The sideways scattering of both reactions exposes geometrical constraints inferring a hydrogen atom emission nearly parallel to the total angular momentum vector, i.e., perpendicularly to the rotational plane of the decomposing complex. These findings are also reflected in the flux contour maps, which contain the overall information on the sideway scattering process (Figure 2C,F).

3. DISCUSSION

With the detection of $C_{10}H_7^{\bullet}$ isomer(s) under single-collision conditions in both the carbon−indene and dicarbon−styrene systems, we are now adjoining these results with electronic structure calculations carried out at an accuracy of ± 10 kJ mol^{-1} to unravel the nature of the isomers formed and to elucidate the underlying reaction mechanisms (Figures 3−6; Supporting Information). Statistical calculations exploiting the Rice−Ramsperger−Kassel−Marcus (RRKM) theory to predict unimolecular reaction rate constants and product branching ratios were also carried out (Supporting Information).

3.1. Carbon−Indene System. For the carbon−indene system, the calculations were conducted on the triplet surface, revealing three product channels (**p1**-**p3**) (Figure 3). A comparison of the experimentally determined reaction energy of −293 ± 34 kJ mol^{-1} with the calculated reaction exoergicities suggests that at least the thermodynamically most stable 2-/1-naphthyl radicals (**p1**/**p2**; X^2A'; Δ_rG = −252/251 ± 10 kJ mol^{-1}) are formed. Formation of the 4-azulenyl isomer (**p3**; Δ_rG = −123 ± 10 kJ mol^{-1}) carrying a fused five- and seven-membered ring might be masked in the low-energy section of $P(E_T)$ and cannot be excluded at the present stage. Note that the computed reaction energies leading to 1- and 2-naphthyl of −251 ± 10 and −252 ± 10 kJ mol^{-1} agree well with the predicted experimental enthalpies of formation from Active Thermochemical Tables (ATcT)[32] of −261 ± 2 and −262 ± 2 kJ mol^{-1}, respectively. These results, combined with the reaction energies obtained from an experimental value of −293 ± 34 kJ mol^{-1}, support the identification of the 1-/2-naphthyl in the carbon−indene system.

Which are the dominating reaction mechanisms for the gas-phase preparation of the 1-/2-naphthyl radicals plus atomic hydrogen? The bimolecular reaction of ground-state triplet atomic carbon with indene is initiated through barrierless additions to the π electronic system of the five-membered ring or the benzene moiety, leading to intermediates **i1**, **i5**, or **i7**, which are stabilized by 215, 67, or 66 kJ mol^{-1} with respect to the separated reactants, respectively. Intermediates **i5** and **i7** are connected via **i6** (a tricyclic structure) through low-lying transition states ranging well below the energy of the separated reactants. Collision complex **i1** can undergo ring opening of the annulated three-membered circle to triplet **i2**, thus forming a naphthalene carbon skeleton. The collision complexes **i5** and **i1** interconnect through a barrier of only 8 kJ mol^{-1}; this pathway should dominate compared to the **i5** → **i6** isomerization, which requires a barrier of 24 kJ mol^{-1} to be overcome. Once accessed, **i2** can undergo a facile unimolecular decomposition via atomic hydrogen elimination from the CH_2 moiety to **p1** or isomerize via a hydrogen shift from the CH_2 moiety to the neighboring CH group to **i3** followed by consecutive isomerization to triplet **i4** (naphthalene). Intermediates **i3** and **i4** can decompose to **p1** and/or **p2** plus atomic hydrogen via three exit channels: **i3** → **p1** + H, **i4** → **p1** + H, and **i4** → **p2** + H with exit transition states located 19, 28, and 24 kJ mol^{-1} above the energy of the separated products. It should be noted that addition pathways of atomic carbon across distinct chemically inequivalent carbon−carbon bonds of the benzene moiety were also located (Supporting Information). These processes lead via ring opening and atomic hydrogen loss to **p4** and **p5**, carrying an adjacent five- and seven-membered ring with the radical center located at the seven-membered ring structure (Figure S4). The energetics of

https://doi.org/10.1021/jacs.5c15459
J. Am. Chem. Soc. 2025, 147, 47359−47369

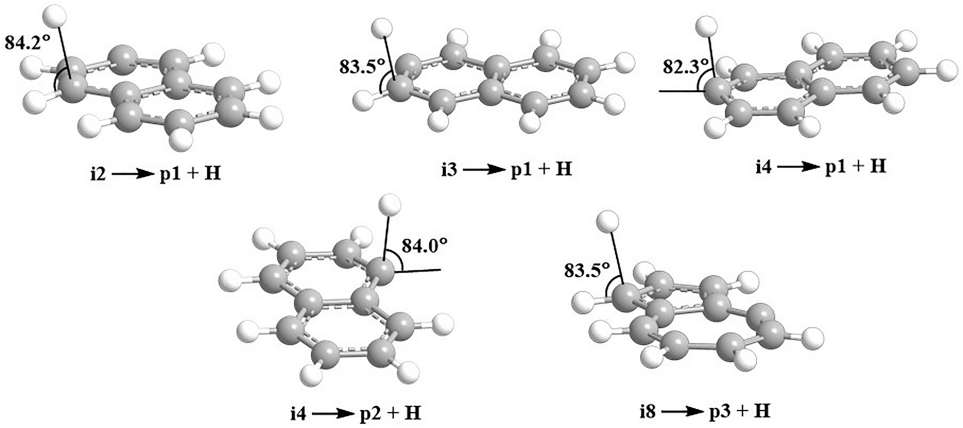

Figure 4. Exit transition states leading to **p1**-**p3**. The angle for each emitting hydrogen atom is given with respect to the rotational plane of the decomposing complex.

these reaction sequences (**i9** → **i10** → **p4** + H, **i11** → **i12** → **p5** + H) exhibit similar behaviors comparing to **i7** → **i8** → **p3** + H. Overall, the electronic structure calculations revealed barrierless pathways to the 1- and 2-naphthyl radicals (X^2A') under single-collision conditions in the atomic carbon−indene system via indirect scattering dynamics with **p1** (2-naphthyl) accessible via decomposition of intermediates **i2, i3**, and **i4** and **p2** (1-naphthyl) exclusively from **i4**.

Which of these isomers dominates? Statistical RRKM (Rice−Ramsperger−Kassel−Marcus) theory is utilized to predict the branching ratios of the $C_{10}H_7^{\bullet}$ isomer (**p1**-**p3**). These calculations are conducted for three different scenarios commencing exclusively with initial intermediates of **i1**, **i5**, or **i7** within the limit of a complete energy randomization. The ultimate branching ratios depend strongly on the initial collision complex. At an experimental collision energy of 36 kJ mol^{-1}, **i7** decomposes predominantly to **p3** with a small fraction of 0.16% dissociating to **p1** (Table S2). In those trajectories where the bimolecular collision between atomic carbon and indene leads to **i1** and **i5**, **p1** will be the highly prevailing product (99.99 and 99.84%, respectively) formed under our experimental condition. Furthermore, the computed geometries of the exit transition states leading to **p1**-**p3** plus H (**i2** → **p1** + H, **i3** → **p1** + H, **i4** → **p1** + H, **i4** → **p2** + H, and **i8** → **p3** + H) from **i2**, **i3**, **i4** and **i8** reveal that the atomic hydrogen is emitted nearly perpendicular to the plane of the rotating complex at angles from 82.3° to 84.2° (Figure 4), which is consistent with the sideway scattering fitting of the $T(\theta)$ distributions.

In conclusion, the formation of the 2-naphthyl radical (**p1**) proceeds via initial collision complexes **i1**, **i5**, and **i6**, with the latter two complexes eventually isomerizing to **i1.** This intermediate ring opens to **i2**, which contains the naphthalene carbon skeleton followed by atomic hydrogen loss and aromatization from the methylene moiety to the 2-naphthyl radical (Figure 3).

3.2. Dicarbon−Styrene System. For the dicarbon−styrene system, both the singlet and triplet $C_{10}H_8$ surfaces were explored (Figure 5A,B). It should be noted that the reaction energies of −363 ± 23 kJ mol^{-1} and −371 ± 23 kJ mol^{-1} for dicarbon reactants in their $X^1\Sigma_g^+$ ground state and $a^3\Pi_u$ excited state, respectively, extracted from experiment closely match the computed values for the formation of 1-/2-naphthyl, −349/-350 ± 10 kJ mol^{-1} for singlet and −359/-361 ± 10 kJ mol^{-1} for triplet, and the reaction energies derived from the enthalpies of formation from ATcT (−356/-357 and −363/-364 ± 2 kJ mol^{-1}), respectively.[32] On the singlet surface, the reaction is initiated via barrierless additions of the dicarbon molecule to the π electron density of the benzene or vinyl moiety accessing collision complexes **i3'** and/or **i1'** (benzene ring) and/or **i2'** (vinyl group). All collision complexes can isomerize via ring closure to the bicyclic intermediate **i4'**. An exotic transition state involving a hydrogen migration and ring closure connects **i1'** to tricyclic intermediate **i7'** through a significant barrier of 197 kJ mol^{-1}; ring opening restores the benzene moiety and a hydrogenated four-carbon side chain (**i9'**). A hydrogen migration from the benzene moiety to the side chain accompanied by hydrogen migration accesses the naphthalene intermediate (**i15'**), which represents the global minimum of the $C_{10}H_8$ potential energy surface. Considering the collision complex **i2'**, a hydrogen shift from the CH_2 group to the terminal carbon of the side chain leads to phenylvinylacetylene (**i8'**), which can undergo ring closure to **i12'**. Alternatively, a hydrogen migration in **i3'** connects to ortho-vinylethynyl benzene (**i6'**), which can subsequently undergo ring closure to a bicyclic carbene intermediate (**i13'**). Inspecting **i4'**, its isomerization via ring contraction provides the three-membered ring intermediate **i11'**, which can undergo ring opening to **i15'**. Second, **i4'** is connected to **i5'** via ring expansion. This opens three routes: (i) an energetically unfavorable rearrangement via a significant barrier of 240 kJ mol^{-1} accessing the azulene intermediate **i14'** followed by H elimination from the five- or seven-membered ring to **p6** or **p5** through loose transition states; (ii) a ring contraction to the tricyclic intermediate **i10'**, which can subsequently isomerize to **i15'** via ring opening of the annulated three-membered cycle; (iii) molecular hydrogen atom loss from the CH_2 group and the bridging carbon to **p7**. These intermediates can undergo multiple unimolecular decomposition pathways via atomic hydrogen loss. The 2-naphthyl radical (**p1**) can be accessed from **i15'** and **i12'** via loose and tight exit transition states, respectively; the 1-naphthyl radical (**p2**) could be generated from **i15'** and **i13'** also via loose and tight exit transition states, respectively.

On the triplet surface, the dicarbon molecule can add barrierlessly to the terminal carbon atom of the side chain and the benzene moiety of the styrene, forming initial intermediates **i16'** and **i17'** lying 198 and 125 kJ mol^{-1} below the separated reactants, respectively. Subsequent isomerization of the initial intermediates involves ring closure leads to **i18'**

https://doi.org/10.1021/jacs.5c15459
J. Am. Chem. Soc. 2025, 147, 47359−47369

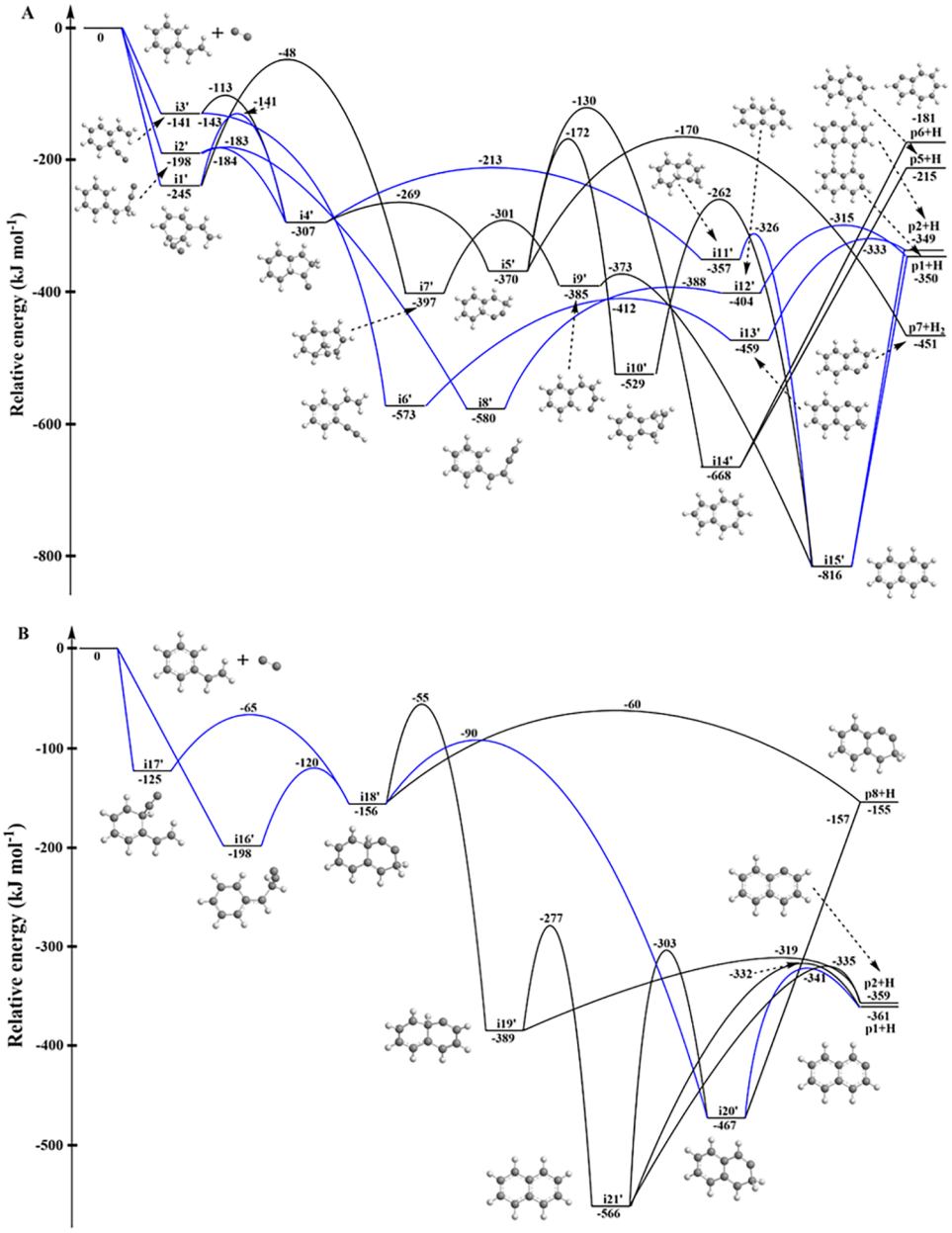

Figure 5. Singlet (A) and triplet (B) PES for the reaction of dicarbon (C_2, $X^1\Sigma_g^+/a^3\Pi_u$) with styrene (C_8H_8, X^1A'). The pathways highlighted in blue represent the dominant routes to naphthyl radicals.

which opens three new routes: (i) unimolecular decomposition via H elimination from the bridging carbon to **p8**; (ii) H migration from the bridging carbon to the neighboring position forming **i20'** which can lose an atomic hydrogen from the CH group via a loose transition state to **p8** or from the CH_2 group to **p1** through a tight transition state located 20 kJ mol^{-1} above the separated products; (iii) H migration from the CH_2 group to the neighboring position leading to **i19'**, which can undergo further H migration to **i21'** (naphthalene), the most stable intermediate on the triplet PES, or directly access **p2** with atomic hydrogen elimination originating from the bridging carbon. Once formed, a 2,3-hydrogen migration in **i21'** connects it to **i20'** via a high barrier lying 164 kJ mol^{-1} above **i20'**, and the decomposition of **i21'** forms **p1** and **p2** via tight exit transition states lying 29 and 24 kJ mol^{-1} above the separated products. Note that the reaction of dicarbon with benzene was previously studied,[33] revealing the formation of the phenylethynyl radical (C_6H_5CC, X^2A') on both singlet and triplet surfaces. According to the calculations, on the singlet surface, dicarbon (C_2, $X^1\Sigma_g^+$) added to a carbon−carbon double bond, leading to the methylidynecyclopropyl benzene followed by non-RRKM unimolecular decomposition to phenylethynyl (C_6H_5CC) plus atomic hydrogen. Recall that in the dicarbon−styrene reaction on the singlet surface, the similar addition mechanism leads to **i1'**. However, the existence of the vinyl moiety in **i1'** results in the distinct reaction dynamics, i.e., **i1'** is identified to undergo ring closure to bicyclic **i4'** or tricyclic **i7'** instead of the formation of ethynylstyryl ($C_2H_3C_6H_4CC$). Similarly, on the triplet surface, the addition of dicarbon (C_2, $a^3\Pi_u$) to one carbon of the benzene molecule (C_2-C_6H_6) or the benzene moiety of styrene (C_2-C_8H_8) forms ethynylbenzene (C_6H_6CC) or ethynylstyrene (C_8H_8CC, **i17'**), respectively. Here, the influence of the vinyl moiety in styrene is also depicted in the subsequent ring

https://doi.org/10.1021/jacs.5c15459
J. Am. Chem. Soc. 2025, 147, 47359−47369

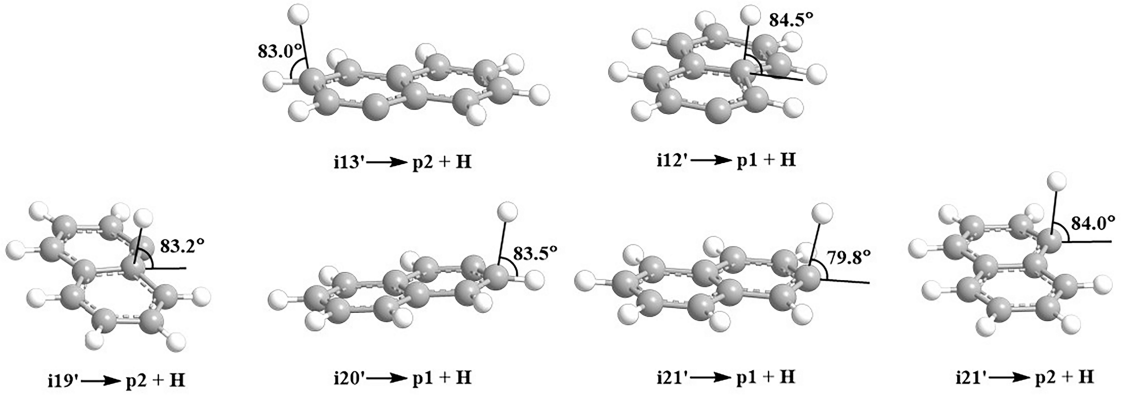

Figure 6. Exit transition states leading to 2-naphthyl (**p1**) and 1-naphthyl (**p2**) radicals. The angle for each emitting hydrogen atom is given with respect to the rotational plane of the decomposing complex.

closure to a bicyclic **i18'** isomer rather than the simple H elimination to ethynylstyryl ($C_2H_3C_6H_4CC$).

It is interesting to compare the RRKM branching ratios for the C_2-C_8H_8 system on the singlet surface with those on the triplet surface (Tables S3 and S4). On the singlet surface, the branching ratios depend strongly on the initial collision complex(es). RRKM calculations reveal that **p1** will be the dominant product if **i1'** and **i2'** are formed (67.3% for **i1'** and 94.0% for **i2'**), 32.3% of **i1'** and 5.9% of **i2'** also decompose to **p2**; and **p2** is almost the only product from **i3'** (99.6%). On the triplet surface, since both **i16'** and **i17'** will isomerize to **i18'**, the formation of **i16'** and **i17'** leads to the same ratios of the final products: 97.7% of them decompose to **p1**, with the remaining 2.3% connecting to **p2**. Thus, on both singlet and triplet surfaces, our calculations predict the almost exclusive synthesis of naphthyl radicals (**p1** and/or **p2**), which is in line with the experiments. These findings are fully supported by the geometry calculations of the exit transition states leading to naphthyl radicals on both singlet (**i13'** and **i12'**) and triplet (**i19'**, **i20'** and **i21'**) surfaces which reveal that the hydrogen atoms are emitted at angles from 80° to 85° relative to the rotation plane of the complexes (Figure 6).

Last, the experimental findings of the isotopic substitution studies can be addressed (Figure S2). For the reaction of singlet dicarbon with D3-styrene ($C_6H_5C_2D_3$, hydrogen and deuterium atoms are color-coded in gray and light blue, respectively, in Figure S2), the formation of **i13'** will only lead to the atomic deuterium loss exit channel (from vinyl) to **p2**, whereas the formation of **i12'** leads to **p1** + H. Moreover, **i15'** can eliminate atomic hydrogen (benzene ring) and atomic deuterium (vinyl moiety) to **p1** or **p2** with a ratio of 1:1 or 3:1, respectively. For the reaction of singlet dicarbon with D5-styrene ($C_6D_5C_2H_3$, hydrogen and deuterium atoms are color-coded in light blue and gray, respectively, in Figure S2), the formation of **i13'** will result in atomic hydrogen elimination from vinyl group to **p2**, **i12'** will undergo deuterium loss to **p1**; and the formation of **i15'** will lead to both atomic hydrogen and deuterium loss to **p1** or **p2** with H/D ratios of 1:1 and 1:3, respectively. In the triplet dicarbon−D3/D5-styrene ($C_6H_5C_2D_3/C_6D_5C_2H_3$) reactions (Figure S2B), it is clear that the formation of **i19'** will lead to **p2**+H in the C_2-D3-styrene system and **p2**+D in the C_2-D5-styrene system, whereas **i20'** or **i21'** can lose a deuterium atom and/or a hydrogen atom to naphthyl radical (**i20'**→**p1**+H/D, **i21'**→**p1**/**p2**+H/D). We can then conclude that atomic hydrogen can be emitted from the vinyl or phenyl groups on both singlet and triplet surfaces of the C_2-C_8H_8 system, in excellent agreement with our experimental predictions.

Overall, on the singlet surface of the C_2-C_8H_8 reaction, four pathways of **i8'**→**i12'**→**p1**+H, **i4'**→**i11'**→**i15'**→**p1**+H, **i4'**→**i11'**→**i15'**→**p2**+H, and **i6'**→**i13'**→**p2**+H can be important in forming 1/2-naphthyl radicals (Figure 5A); their formation involves distinct collision complexes **i1'**-**i3'**. The triplet surface is simpler, and the formation of **i18'** is central for accessing the dominant reaction pathway **i18'**→**i20'**→**p1**+H with **i18'** connected to both initial intermediates of **i16'** and **i17'** (Figure 5B).

3.3. Astrochemical Modeling. The identification of the barrierless formation of 1/2-naphthyl radicals ($C_{10}H_7^{\bullet}$) through two neutral−neutral reactions provides an opportunity to explore the aromatic chemistry deep inside the photon-shielded dense molecular clouds. To investigate the implications of our laboratory results, we explore an enhanced neutral−neutral chemical reaction network, which incorporates the newly identified reactions of ground-state carbon (C) with indene (C_9H_8) and of dicarbon (C_2) with styrene (C_8H_8) and excludes photodissociation. The details of the astrochemical modeling based on the UMIST (University of Manchester Institute for Science and Technology) database have been presented before.[34−36]

As depicted in Figure 7, the modeling studies reveal that even in the darkest cold molecular cloud, the naphthyl radicals ($C_{10}H_7$) can be efficiently formed with predicted peak fractional abundances of 1.8×10^{-10} with respect to molecular hydrogen (H_2) at 6.3×10^5 years. Reactions 1 (C + C_9H_8 → $C_{10}H_7$ + H) and 2 (C_2 + C_8H_8 → $C_{10}H_7$ + H) contribute 96 and 4%, respectively. Furthermore, larger PAHs of anthracene/phenanthrene ($C_{14}H_{10}$) are suggested to be formed through reaction with vinylacetylene (C_4H_4)[8] with a peak fractional abundance of at least 4.0×10^{-11} with respect to molecular hydrogen. Considering that o-C_6H_4 (benzyne) has been detected recently with fractional abundances of $(5.0 \pm 1.0) \times 10^{-11}$ in the cold molecular cloud TMC-1 via the Yebes 40m radio telescope,[37] the predicted fractional abundances here suggest that the naphthyl radicals formed in photon-shielded dense molecular clouds are a promising candidate for future astronomical observations.

4. CONCLUSIONS

Our combined crossed molecular beam experiments and electronic structure calculations exposed a novel concept on

https://doi.org/10.1021/jacs.5c15459
J. Am. Chem. Soc. 2025, 147, 47359−47369

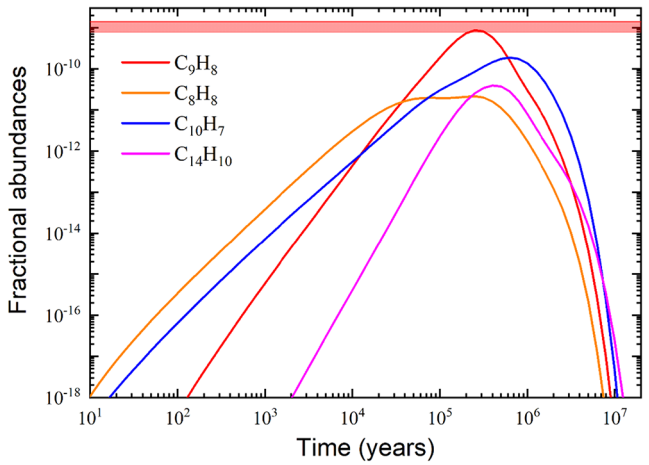

Figure 7. Fractional abundances of the styrene (C_8H_8, orange), indene (C_9H_8, red), naphthyl ($C_{10}H_7$, blue), and anthracene/phenanthrene ($C_{14}H_{10}$, magenta) are plotted as a function of time. Astronomically observed fractional abundances along with the uncertainties of indene are visualized by the horizontal bars.

the low-temperature gas-phase synthesis of naphthyl radicals ($C_{10}H_7^{\bullet}$)—the simplest prototype of polycyclic aromatic hydrocarbon radical—inside photon-shielded cold molecular clouds such as the Taurus Molecular Cloud (TMC-1). The formation of naphthyl radicals has been tentatively studied before. In the laboratory, naphthyl radical can be prepared in a single-crystal naphthalene matrix undergoing radioactive decay,[38,39] or via photodissociation of di-1-naphthoylperoxide (DNPO) or thermolysis of 1,2-diethynylbenzene in solution.[40,41] In a flow reactor, naphthyl radicals might be formed as minor products from the pyrolysis of ethynylbenzene in helium.[42] In combustion conditions, the HACA mechanism predicts that 1-naphthyl radical might be produced with a barrier of around 37 kJ mol^{-1}, and 1- and 2-naphthyl radicals are mainly formed via the H atom abstraction of naphthalene.[9,43,44] Furthermore, the calculation also predicts that naphthyl can be formed from phenylacetylene via the ethynyl addition mechanism (EAM).[45] However, barrierless gas-phase pathways to naphthyl have still been elusive. Here, the barrierless bimolecular reactions of atomic carbon (C) with indene (C_9H_8) and of dicarbon molecule (C_2) with styrene (C_8H_8) are driven by ring expansion and cyclization, respectively, together with aromatization to eventually form 1- and 2-naphthyl radicals in single-collision events of bimolecular reactions involving readily available reactants. The reactants include indene identified as the most abundant aromatic and organic ring molecule to date in TMC-1 with fractional abundance of $(0.8-1.4) \times 10^{-9}$ relative to H_2 and styrene predicted with the upper limit of fractional abundance of 10^{-8} in TMC-1.[46,47] Considering that the hydrogen atom of the aromatic ring of the styrene and indene reactants can be replaced with any organic group, these bimolecular gas-phase reactions represent a universal template toward the formation of substituted naphthyl radicals. These facile routes challenge conventional wisdom that aromatic radicals are formed in deep space solely via "bright" gas-phase photochemistry of their closed-shell polycyclic aromatic hydrocarbon (PAH) precursors. A hitherto disregarded "dark" aromatic radical chemistry with aromatic radicals synthesized in the gas phase via chemical reactions rather than a "bright" photochemistry offers a new concept on the chemical evolution of the chemistry of dark molecular clouds, thus facilitating a better understanding of the origin and chemical evolution of carbon in our aromatic Universe.

5. EXPERIMENTAL AND COMPUTATIONAL SECTION

5.1. Experimental Methods—Carbon−Indene System. The gas-phase bimolecular reaction of ground-state carbon (C, ^3P) with indene (C_9H_8, X^1A') was investigated under single-collision conditions employing the crossed molecular beam (CMB) scattering technique with mass spectrometric detection in the time-of-flight (TOF) mode.[48,49] Briefly, the supersonic beam of ground-state carbon atoms was prepared using a laser ablation source by ablating a rotating graphite rod with a Nd:YAG laser (266 nm, 10−12 mJ pulse^{-1}, 30 Hz) and seeding the ablated carbon atoms in a helium carrier (4 atm) released by a piezoelectric valve at 60 Hz. The atomic carbon beam was skimmed and velocity selected by a chopper wheel operating at 120 Hz. Peak velocity and speed ratio of the chopped section of the primary beam were 2538 ± 46 m s^{-1} and 2.8 ± 0.3, respectively. In this manner, carbon atoms are produced only in the ground ^3P state. The indene (TCI, > 99%) reactant was held in a bubbler and seeded in krypton (550 Torr, Praxair, 99.999%), and the supersonic beam was released by the second piezoelectric valve with the peak velocity and speed ratio of 367 ± 6 m s^{-1} and 15.2 ± 1.4, respectively. Two beams of the reactants are crossed at 90° in the interaction region under single-collision conditions, leading to a collision energy of 35.8 ± 1.2 kJ mol^{-1} and a center-of-mass angle of 54.4 ± 0.5°. Experimental conditions were optimized to make sure that the primary beam contains only a small amount of dicarbon (<5% compared to atomic carbon).

5.2. Experimental Methods—Dicarbon−Styrene System. Dicarbon beam [C_2 ($X^1\Sigma_g^+/a^3\Pi_u$)] was generated by the same ablation source described above. The 266 nm laser output at an energy of 9−11 mJ pulse^{-1} and 4 atm Neon carrier (Ne, 99.9999%) was used. Experimental conditions and time sequences were optimized to maximize the dicarbon concentrations in the supersonic beam. The ro-vibrational distribution of both singlet ground state ($X^1\Sigma_g^+$) and the lowest lying triplet state ($a^3\Pi_u$) of the dicarbon beam was characterized by laser-induced fluorescence (LIF).[50] In detail, the $X^1\Sigma_g^+$ state was probed via the Mulliken excitation ($D^1\Sigma_u^+$-$X^1\Sigma_g^+$) and the bimodal rotational distributions of both $v = 0$, 1 were confirmed at fractions of 0.83 ± 0.10 (200 K: 0.44 ± 0.05; 1000 K: 0.39 ± 0.05) and 0.17 ± 0.04 (200 K: 0.06 ± 0.02; 1000 K: 0.11 ± 0.02). The rotational temperature (T_{rot}) for the first and second vibrational levels of the $a^3\Pi_u$ state was detected to be 240 ± 30 and 190 ± 30 K via the Swan band transition ($d^3\Pi_g$-$a^3\Pi_u$) with fractions of 0.67 ± 0.05 and 0.33 ± 0.05, respectively.[50] A stainless-steel bubbler was used to hold the styrene reactant and krypton carrier introduced at 550 Torr during the reaction. The corresponding peak velocity of 372 ± 6 m s^{-1} and the speed ratio of 12.8 ± 0.6 of the styrene beam were determined, resulting in a collision energy of 20.6 ± 0.5 kJ mol^{-1} and a center-of-mass angle of 48.9 ± 0.4° in the C_2−C_8H_8 reaction (Table S1). In addition, the D3- and D5-styrene (CDN Isotopes, 99% D), i.e., $C_6H_5C_2D_3$ and $C_6D_5C_2H_3$, were employed to confirm the position of the hydrogen atom elimination.

For both reactions, the neutral scattered products entering the triply differentially pumped, ultrahigh vacuum (6.6×10^{-12} Torr) detector were ionized via an electron impact ionizer, and the laboratory data were mass-selected via a quadrupole mass spectrometer operating in the TOF mode. The details of our detector have been depicted elsewhere.[51] In brief, the selected ions initiate a cascade-of-electron pulse by using a target biased at −22.5 kV and generate a photon pulse from an organic scintillator is generated. Finally, a Burle photomultiplier tube (−1.35 kV), a discriminator operating at 1.6 mV and a multichannel scaler were utilized. The detector unit is rotatable within the plane of the two beams, and the laboratory data were collected at distinct angles. To obtain the LAD of selected m/z, the integrated TOF spectra signal collected are normalized with respect to the signal at the CM angle. The laboratory data, including the LAD and TOF spectra, were transformed into the

https://doi.org/10.1021/jacs.5c15459
J. Am. Chem. Soc. 2025, 147, 47359−47369

CM frame using a forward-convolution routine for the underlying reaction dynamics. The CM translational energy ($P(E_T)$) and angular ($T(\theta)$) flux distributions are varied iteratively before a best fit of the laboratory data is derived. $I(u, \theta) \sim P(u) \times T(\theta)$, the reactive differential cross section with the product intensity (I) as a function of the velocity u and the CM angle θ, reveals an overall image of the reaction.[29]

5.3. Computational Section. Electronic structure calculations in the present work were carried out on the $C_{10}H_8$ potential energy surfaces accessed by the carbon−indene (triplet) and dicarbon−styrene (singlet and triplet) reactions. In particular, geometries of the reactants, products, intermediates, and transition states involved in these reactions were optimized at the density functional theory ωB97X-D/6−311G(d,p) level (Table S4),[52,53] with vibrational frequencies and zero-point vibrational energies (ZPE) computed using the same theoretical approach. Single-point energies were further refined within the explicitly correlated CCSD(T)-F12/cc-pVTZ-F12 method[54,55] with ZPE(ωB97X-D/6−311G(d,p)) included, which normally provides the energetic parameters of local minima and transition states within "chemical accuracy" of ∼5−10 kJ mol^{-1} for hydrocarbons in terms of average absolute deviations.[56] The GAUSSIAN 16[57] and MOLPRO 2021[58] program packages were used for the ab initio calculations. The Rice−Ramsperger−Kassel−Marcus (RRKM) theory[59,60] implemented in our Unimol code[61] was applied to compute energy-dependent rate constants of all unimolecular reaction steps on the $C_{10}H_8$ singlet and triplet surfaces. For H loss steps on the singlet $C_{10}H_8$ surface accessed by the styrene + $C_2(X^1\Sigma_g^+)$ reaction, which occur without distinct exit transition states, energy-dependent rate constants were computed using the micro-canonical variational transition state theory μ-VTST. Here, the H loss potential energy surfaces (PES) were scanned at the ωB97X-D/6−311G(d,p) level of theory along the reaction coordinate represented by the length of the breaking C−H bonds. Vibrational frequencies for each optimized structure along the PES scan were computed at the same level of theory with the projection of the reaction coordinate out. The ωB97X-D/6−311G(d,p) relative energies of these structures were scaled by a factor chosen to match the ωB97X-D/6−311G(d,p) relative energy of the $C_{10}H_7$ + H products to its value obtained at the highest CCSD(T)-F12/cc-pVTZ-F12 level. The optimized structures along the PES profile were considered variational transition state (VTS) candidates. The unimolecular rate constants for the barrierless H loss were evaluated for each VTS candidate using the RRKM formalism, and the minimal rate constant was then selected. Next, product branching ratios at the zero-pressure limit under single-collision conditions were assessed within the steady-state approximation.[59,60] Assuming single-collision conditions, master equations for unimolecular reactions can be expressed as follows

$$\frac{d[C]_i}{dt} = \sum k_n[C]_i - \sum k_m[C]_j$$

where $[C]_i$ and $[C]_j$ are concentrations of various intermediates and products, respectively, and k_n and k_m are the micro-canonical rate constants for the formation and consumption of each intermediate i, respectively, computed using the RRKM theory. Only a single total-energy level was considered throughout, as for single-collision crossed-beam conditions. In such a case, rate constants of different unimolecular reaction steps are independent of each other, but relative product yields can be determined from the solution of the system of coupled master equations, which is reduced to a system of linear equations within the steady-state approximation, where the concentration of a chosen initial intermediate formed in the bimolecular reaction is taken as a constant and concentrations of all other unimolecular intermediates remain steady, so that their $\frac{d[C]_i}{dt} = 0$.

■ ASSOCIATED CONTENT

Supporting Information

The Supporting Information is available free of charge at https://pubs.acs.org/doi/10.1021/jacs.5c15459.

Explanation of the laboratory and center-of-mass frame, supplementary experimental results, experimental parameters (Table S1); statistical branching ratios for the triplet PES for the C+C_9H_8 reaction (Table S2); singlet PES for the C_2+C_8H_8 reaction (Table S3); the triplet PES for the C_2+C_8H_8 reaction (Table S4); optimized coordinates and calculated vibrational frequencies for stationary structures involved in the C−C_9H_8 reaction (Table S5); C_2 ($X^1\Sigma_g^+$)-C_8H_8 reaction (Table S6) and C_2 ($a^3\Pi_u$)-C_8H_8 reaction (Table S7); structures that might be formed from naphthyl radicals (Figure S1); Newton diagram of a reactive scattering event (Figure S2); cross sections of our universal CMB machine (Figure S3); additional pathways of the C−C_9H_8 reaction (Figure S4); and singlet and triplet PESs of the reactions of C_2 with D3/D5-styrene (Figure S5) (PDF)

■ AUTHOR INFORMATION

Corresponding Authors

Ralf I. Kaiser − *Department of Chemistry, University of Hawai'i at Manoa, Honolulu, Hawaii 96822, United States;* orcid.org/0000-0002-7233-7206; Email: ralfk@hawaii.edu

Alexander M. Mebel − *Department of Chemistry and Biochemistry, Florida International University, Miami, Florida 33199, United States;* orcid.org/0000-0002-7233-3133; Email: mebela@fiu.edu

Xiaohu Li − *Xinjiang Astronomical Observatory, Chinese Academy of Sciences, Urumqi, Xinjiang 830011, China; Xinjiang Key Laboratory of Radio Astrophysics, Urumqi, Xinjiang 830011, China; Key Laboratory of Radio Astronomy and Technology, Chinese Academy of Sciences, Beijing 100101, China*; Email: xiaohu.li@xao.ac.cn

Authors

Zhenghai Yang − *Department of Chemistry, University of Hawai'i at Manoa, Honolulu, Hawaii 96822, United States;* Present Address: State Key Laboratory of Precision Spectroscopy, East China Normal University, Shanghai 200062, China

Galiya R. Galimova − *Department of Chemistry and Biochemistry, Florida International University, Miami, Florida 33199, United States*

Chao He − *Department of Chemistry, University of Hawai'i at Manoa, Honolulu, Hawaii 96822, United States*

Shane J. Goettl − *Department of Chemistry, University of Hawai'i at Manoa, Honolulu, Hawaii 96822, United States;* orcid.org/0000-0003-1796-5725

Complete contact information is available at: https://pubs.acs.org/10.1021/jacs.5c15459

Notes

The authors declare no competing financial interest.

■ ACKNOWLEDGMENTS

This work was supported by the U.S. Department of Energy, Basic Energy Sciences, by Grant No. DE-FG02-03ER15411 to

the University of Hawaii at Manoa and No. DE-FG02-04ER15570 to the Florida International University.

REFERENCES

(1) Micelotta, E. R.; Jones, A. P.; Tielens, A. G. G. M. Polycyclic aromatic hydrocarbon processing in a hot gas. *Astron. Astrophys.* **2010**, *510*, No. A37.
(2) Tielens, A. G. G. M. The molecular universe. *Rev. Mod. Phys.* **2013**, *85*, 1021−1081.
(3) Frenklach, M.; Feigelson, E. D. Formation of polycyclic aromatic hydrocarbons in circumstellar envelopes. *Astrophys. J.* **1989**, *341*, 372−384.
(4) Zenobi, R.; Philippoz, J.-M.; Zare, R. N.; Buseck, P. R. Spatially resolved organic analysis of the Allende meteorite. *Science* **1989**, *246*, 1026−1029.
(5) Tielens, A. G. G. M. Interstellar polycyclic aromatic hydrocarbon molecules. *Annu. Rev. Astron. Astrophys.* **2008**, *46*, 289−337.
(6) Kaiser, R. I.; Hansen, N. An aromatic universe−a physical chemistry perspective. *J. Phys. Chem. A* **2021**, *125*, 3826−3840.
(7) Parker, D. S. N.; Zhang, F.; Kim, Y. S.; Kaiser, R. I.; Landera, A.; Kislov, V. V.; Mebel, A. M.; Tielens, A. Low temperature formation of naphthalene and its role in the synthesis of PAHs (polycyclic aromatic hydrocarbons) in the interstellar medium. *Proc. Natl. Acad. Sci. U.S.A.* **2012**, *109*, 53−58.
(8) Zhao, L.; Kaiser, R. I.; Xu, B.; Ablikim, U.; Ahmed, M.; Evseev, M. M.; Bashkirov, E. K.; Azyazov, V. N.; Mebel, A. M. Low-temperature formation of polycyclic aromatic hydrocarbons in Titan's atmosphere. *Nat. Astron.* **2018**, *2*, 973−979.
(9) Mebel, A. M.; Landera, A.; Kaiser, R. I. Formation mechanisms of naphthalene and indene: From the interstellar medium to combustion flames. *J. Phys. Chem. A* **2017**, *121*, 901−926.
(10) Zhao, L.; Kaiser, R. I.; Xu, B.; Ablikim, U.; Ahmed, M.; Evseev, M. M.; Bashkirov, E. K.; Azyazov, V. N.; Mebel, A. M. A unified mechanism on the formation of acenes, helicenes, and phenacenes in the gas phase. *Angew. Chem.* **2020**, *132*, 4080−4087.
(11) Parker, D. S. N.; Kaiser, R. I.; Bandyopadhyay, B.; Kostko, O.; Troy, T. P.; Ahmed, M. Unexpected chemistry from the reaction of naphthyl and acetylene at combustion-like temperatures. *Angew. Chem., Int. Ed.* **2015**, *54*, 5421−5424.
(12) Hamadi, A.; Sun, W.; Abid, S.; Chaumeix, N.; Comandini, A. An experimental and kinetic modeling study of benzene pyrolysis with C2−C3 unsaturated hydrocarbons. *Combust. Flame* **2022**, *237*, No. 111858.
(13) Mitra, T.; Zhang, T.; Sediako, A. D.; Thomson, M. J. Understanding the formation and growth of polycyclic aromatic hydrocarbons (PAHs) and young soot from n-dodecane in a sooting laminar coflow diffusion flame. *Combust. Flame* **2019**, *202*, 33−42.
(14) Wang, H.; Guan, J.; Xu, G.; Mercier, X.; Zhang, J.; Guo, H.; Yu, T.; Gui, H.; Huang, T.; Truhlar, D. G.; Wang, Z. Resonance-stabilized radical clustering bridges the gap between gaseous precursors and soot in the inception stage. *Proc. Natl. Acad. Sci. U.S.A.* **2025**, *122*, No. e2503292122.
(15) Martin, J. W.; Salamanca, M.; Kraft, M. Soot inception: Carbonaceous nanoparticle formation in flames. *Prog. Energy Combust. Sci.* **2022**, *88*, No. 100956.
(16) Thomson, M. J. Modeling soot formation in flames and reactors: Recent progress and current challenges. *Proc. Combust. Inst.* **2023**, *39*, 805−823.
(17) Wang, H.; Guan, J.; Gao, J.; Zhang, J.; Xu, Q.; Xu, G.; Jiang, L.; Xing, L.; Truhlar, D. G.; Wang, Z. Direct observation of covalently bound clusters in resonantly stabilized radical reactions and implications for carbonaceous particle growth. *J. Am. Chem. Soc.* **2024**, *146*, 13571−13579.
(18) Zeichner, S. S.; Aponte, J. C.; Bhattacharjee, S.; Dong, G.; Hofmann, A. E.; Dworkin, J. P.; Glavin, D. P.; Elsila, J. E.; Graham, H. V.; Naraoka, H.; et al. Polycyclic aromatic hydrocarbons in samples of Ryugu formed in the interstellar medium. *Science* **2023**, *382*, 1411−1416.
(19) Naraoka, H.; Takano, Y.; Dworkin, J. P.; Oba, Y.; Hamase, K.; Furusho, A.; Ogawa, N. O.; Hashiguchi, M.; Fukushima, K.; Aoki, D.; et al. Soluble organic molecules in samples of the carbonaceous asteroid (162173) Ryugu. *Science* **2023**, *379*, No. eabn9033.
(20) Glavin, D. P.; Dworkin, J. P.; Alexander, C. M. O. D.; Aponte, J. C.; Baczynski, A. A.; Barnes, J. J.; Bechtel, H. A.; Berger, E. L.; Burton, A. S.; Caselli, P.; et al. Abundant ammonia and nitrogen-rich soluble organic matter in samples from asteroid (101955) Bennu. *Nat. Astron.* **2025**, *9*, 199−210.
(21) Lauretta, D. S.; Connolly, H. C., Jr; Aebersold, J. E.; Alexander, C. M. O. D.; Ballouz, R. L.; Barnes, J. J.; Bates, H. C.; Bennett, C. A.; Blanche, L.; Blumenfeld, E. H.; et al. Asteroid (101955) Bennu in the laboratory: Properties of the sample collected by OSIRIS-REx. *Meteorit. Planet. Sci.* **2024**, *59*, 2453−2486.
(22) Herbst, E. The chemistry of interstellar space. *Chem. Soc. Rev.* **2001**, *30*, 168−176.
(23) Shingledecker, C. N.; Herbst, E. A general method for the inclusion of radiation chemistry in astrochemical models. *Phys. Chem. Chem. Phys.* **2018**, *20*, 5359−5367.
(24) McGuire, B. A.; Loomis, R. A.; Burkhardt, A. M.; Lee, K. L. K.; Shingledecker, C. N.; Charnley, S. B.; Cooke, I. R.; Cordiner, M. A.; Herbst, E.; Kalenskii, S.; et al. Detection of two interstellar polycyclic aromatic hydrocarbons via spectral matched filtering. *Science* **2021**, *371*, 1265−1269.
(25) Shen, C. J.; Greenberg, J.; Schutte, W.; Van Dishoeck, E. Cosmic ray induced explosive chemical desorption in dense clouds. *Astron. Astrophys.* **2004**, *415*, 203−215.
(26) Willacy, K.; Langer, W. The importance of photoprocessing in protoplanetary disks. *Astrophys. J.* **2000**, *544*, No. 903.
(27) Agúndez, M.; Marcelino, N.; Tercero, B.; Cernicharo, J. Aromatic cycles are widespread in cold clouds. *Astron. Astrophys.* **2023**, *677*, No. L13.
(28) Miller, W. B.; Safron, S. A.; Herschbach, D. R. Exchange Reactions of Alkali Atoms with Alkali Halides: A Collision Complex Mechanism. *Discuss. Faraday Soc.* **1967**, *44*, 108−122.
(29) Levine, R. D. *Molecular Reaction Dynamics*; Cambridge University Press: Cambridge, 2005.
(30) Gu, X.; Guo, Y.; Zhang, F.; Mebel, A. M.; Kaiser, R. I. Reaction Dynamics of Carbon-Bearing Radicals in Circumstellar Envelopes of Carbon Stars. *Faraday Discuss.* **2006**, *133*, 245−275.
(31) Kaiser, R. I. Experimental investigation on the formation of carbon-bearing molecules in the interstellar medium via neutral−neutral reactions. *Chem. Rev.* **2002**, *102*, 1309−1358.
(32) Ruscic, B.; Bross, D. H. Active Thermochemical Tables (ATcT) values based on ver. 1.220 of the Thermochemical Network *Argonne National Laboratory* 2025.
(33) Gu, X.; Guo, Y.; Zhang, F.; Mebel, A. M.; Kaiser, R. I. A crossed molecular beams study of the reaction of dicarbon molecules with benzene. *Chem. Phys. Lett.* **2007**, *436*, 7−14.
(34) Millar, T. J.; Walsh, C.; Van de Sande, M.; Markwick, A. J. The UMIST database for astrochemistry 2022. *Astron. Astrophys.* **2024**, *682*, No. A109.
(35) Yang, Z.; Galimova, G. R.; He, C.; Goettl, S. J.; Paul, D.; Lu, W.; Ahmed, M.; Mebel, A. M.; Li, X.; Kaiser, R. I. Gas-phase formation of the resonantly stabilized 1-indenyl ($C_9H_7^{\bullet}$) radical in the interstellar medium. *Sci. Adv.* **2023**, *9*, No. eadi5060.
(36) Yang, Z.; Medvedkov, I. A.; Goettl, S. J.; Nikolayev, A. A.; Mebel, A. M.; Li, X.; Kaiser, R. I. Low-temperature gas-phase formation of cyclopentadiene and its role in the formation of aromatics in the interstellar medium. *Proc. Natl. Acad. Sci. U.S.A.* **2024**, *121*, No. e2409933121.
(37) Cernicharo, J.; Agúndez, M.; Kaiser, R. I.; Cabezas, C.; Tercero, B.; Marcelino, N.; Pardo, J.; De Vicente, P. Discovery of benzyne, o-C_6H_4, in TMC-1 with the QUIJOTE line survey. *Astron. Astrophys.* **2021**, *652*, No. L9.
(38) Lloyd, R. V.; Wood, D. E. EPR Studies of 1-Naphthyl and 2-Naphthyl Radicals Produced by Tritium Decay. *J. Chem. Phys.* **1970**, *52*, 2153−2154.

https://doi.org/10.1021/jacs.5c15459
J. Am. Chem. Soc. 2025, 147, 47359−47369

(39) Lloyd, R. V.; Wood, D. E. Tritium Decay Synthesis of Free Radicals. An EPR Study of 2-Naphthyl Radical in Single-Crystal Naphthalene-d8. *J. Chem. Phys.* **1972**, *56*, 916−921.
(40) Abel, B.; Aßmann, J.; Buback, M.; Kling, M.; Schmatz, S.; Schroeder, J. Ultrafast decarboxylation of organic peroxides in solution: Interplay of different spectroscopic techniques, quantum chemistry, and theoretical modeling. *Angew. Chem., Int. Ed.* **2003**, *42*, 299−303.
(41) Thoen, K. K.; Thoen, J. C.; Uckun, F. M. Reactivity of 1, 4-didehydronaphthalene toward organic hydrogen atom donors. *Tetrahedron Lett.* **2000**, *41*, 4019−4024.
(42) Guthier, K.; Hebgen, P.; Homann, K. H.; Hofmann, J.; Zimmermann, G. Addition and cyclization reactions in the thermal conversion of hydrocarbons with enyne structure, II. Analysis of radicals and carbenes from ethynylbenzene. *Liebigs Ann.* **1995**, *1995*, 637−644.
(43) Parker, D. S. N.; Kaiser, R. I.; Troy, T. P.; Ahmed, M. Hydrogen abstraction/acetylene addition revealed. *Angew. Chem., Int. Ed.* **2014**, *53*, 7740−7744.
(44) Kislov, V. V.; Sadovnikov, A.; Mebel, A. Formation mechanism of polycyclic aromatic hydrocarbons beyond the second aromatic ring. *J. Phys. Chem. A* **2013**, *117*, 4794−4816.
(45) Mebel, A. M.; Kislov, V. V.; Kaiser, R. I. Photoinduced mechanism of formation and growth of polycyclic aromatic hydrocarbons in low-temperature environments via successive ethynyl radical additions. *J. Am. Chem. Soc.* **2008**, *130*, 13618−13629.
(46) Burkhardt, A. M.; Lee, K. L. K.; Changala, P. B.; Shingledecker, C. N.; Cooke, I. R.; Loomis, R. A.; Wei, H.; Charnley, S. B.; Herbst, E.; McCarthy, M. C. Discovery of the pure polycyclic aromatic hydrocarbon indene (c-C_9H_8) with GOTHAM observations of TMC-1. *Astrophys. J. Lett.* **2021**, *913*, No. L18.
(47) Cernicharo, J.; Fuentetaja, R.; Agúndez, M.; Kaiser, R. I.; Cabezas, C.; Marcelino, N.; Tercero, B.; Pardo, J. R.; de Vicente, P. Discovery of fulvenallene in TMC-1 with the QUIJOTE line survey. *Astron. Astrophys.* **2022**, *663*, No. L9.
(48) Yang, Z.; Galimova, G. R.; He, C.; Doddipatla, S.; Mebel, A. M.; Kaiser, R. I. Gas-phase formation of 1, 3, 5, 7-cyclooctatetraene (C_8H_8) through ring expansion via the aromatic 1, 3, 5-cyclooctatrien-7-yl radical ($C_8H_9^{\bullet}$) transient. *J. Am. Chem. Soc.* **2022**, *144*, 22470−22478.
(49) Yang, Z.; Doddipatla, S.; He, C.; Krasnoukhov, V. S.; Azyazov, V. N.; Mebel, A. M.; Kaiser, R. I. Directed gas phase formation of silene (H_2SiCH_2). *Chem. - Eur. J.* **2020**, *26*, 13584−13589.
(50) Dangi, B. B.; Maity, S.; Kaiser, R. I.; Mebel, A. M. A combined crossed beam and ab initio investigation of the gas phase reaction of dicarbon molecules (C_2; $X^1\Sigma_g^+/a^3\Pi_u$) with propene (C_3H_6; X^1A'): identification of the resonantly stabilized free radicals 1-and 3-vinylpropargyl. *J. Phys. Chem. A* **2013**, *117*, 11783−11793.
(51) Yang, Z.; Fujioka, K.; Galimova, G. R.; Medvedkov, I. A.; Goettl, S. J.; Sun, R.; Mebel, A. M.; Kaiser, R. I. Directed Gas-Phase Formation of Azulene ($C_{10}H_8$): Unraveling the Bottom-Up Chemistry of Saddle-Shaped Aromatics. *ACS Cent. Sci.* **2025**, *11*, 322−330.
(52) Becke, A. D. Density-functional thermochemistry. III. the role of exact exchange. *J. Chem. Phys.* **1993**, *98*, 5648−5652.
(53) Lee, C.; Yang, W.; Parr, R. G. Development of the Colle-Salvetti correlation-energy formula into a functional of the electron density. *Phys. Rev. B* **1988**, *37*, No. 785.
(54) Adler, T. B.; Knizia, G.; Werner, H.-J. A simple and efficient CCSD (T)-F12 approximation. *J. Chem. Phys.* **2007**, *127*, No. 221106.
(55) Knizia, G.; Adler, T. B.; Werner, H.-J. Simplified CCSD(T)-F12 methods: Theory and benchmarks. *J. Chem. Phys.* **2009**, *130*, No. 054104.
(56) Zhang, J.; Valeev, E. F. Prediction of reaction barriers and thermochemical properties with explicitly correlated coupled-cluster methods: a basis set assessment. *J. Chem. Theory Comput.* **2012**, *8*, 3175−3186.
(57) Frisch, M. J.; Trucks, G. W.; Schlegel, H. B.; Scuseria, G. E.; Robb, M. A.; Cheeseman, J. R.; Scalmani, G.; Barone, V.; Mennucci, B.; Petersson, G. A.et al. *Gaussian 16*; Gaussian Inc.: Wallingford, CT, 2019.
(58) Werner, H. J.; Knowles, P. J.; Lindh, R.; Manby, F. R.; Schütz, M.; Celani, P.; Korona, T.; Rauhut, G.; Amos, R.; Bernhardsson, A.et al. MOLPRO. In *Version 2021.2, A Package of Ab Initio Programs*; University of Cardiff: Cardiff, UK, 2021.
(59) Holbrook, K. A.; Pilling, M. J.; Robertson, S. H. *Unimolecular Reactions*, 2nd ed.; Wiley-Interscience: London and New York, 1996.
(60) Kislov, V. V.; Nguyen, T. L.; Mebel, A. M.; Lin, S. H.; Smith, S. C. Photodissociation of benzene under collision-free conditions: An ab initio/Rice−Ramsperger−Kassel−Marcus study. *J. Chem. Phys.* **2004**, *120*, 7008−7017.
(61) He, C.; Zhao, L.; Thomas, A. M.; Morozov, A. N.; Mebel, A. M.; Kaiser, R. I. Elucidating the chemical dynamics of the elementary reactions of the 1-propynyl radical (CH_3CC; X^2A_1) with methylacetylene (H_3CCCH; X^1A_1) and allene (H_2CCCH_2; X^1A_1). *J. Phys. Chem. A* **2019**, *123*, 5446−5462.

https://doi.org/10.1021/jacs.5c15459
J. Am. Chem. Soc. 2025, 147, 47359−47369